

AN EXPLICIT UPDATE SCHEME FOR INVERSE PARAMETER
AND INTERFACE ESTIMATION OF PIECEWISE CONSTANT
COEFFICIENTS IN LINEAR ELLIPTIC PDES*JAN HEGEMANN[†], ALEJANDRO CANTARERO[‡], CASEY L. RICHARDSON[§], AND
JOSEPH M. TERAN[‡]

Abstract. We introduce a general and efficient method to recover piecewise constant coefficients occurring in elliptic partial differential equations as well as the interface where these coefficients have jump discontinuities. For this purpose, we use an output least squares approach with level set and augmented Lagrangian methods. Our formulation incorporates the inherent nature of the piecewise constant coefficients, which eliminates the need for a complicated nonlinear solve at every iteration. Instead, we obtain an explicit update formula and therefore vastly speed up computation. We employ our approach to the example problems of Poisson's equation and linear elasticity and provide the combination of simultaneously recovering coefficients and interface.

Key words. inverse problems, elliptic problems, inverse parameter estimation, inverse geometric problems, Poisson's equation, linear elasticity, augmented Lagrangian method, level set method

AMS subject classifications. 65N21, 65N20, 65K10, 49M05

DOI. 10.1137/110834500

1. Introduction. The identification of coefficients occurring in elliptic partial differential equations (PDEs) is a problem that arises in several different fields, including solid and fluid mechanics, image processing, and many more (see, e.g., [48]). In the case of medical imaging, inverse parameter estimation could potentially be used to determine the properties and location of different tissue types while using minimally invasive technologies (see [46] and references therein) as an alternative to major surgery. Classifying the elastic properties of tissue and locating abnormalities can help to identify and pinpoint cancerous growth [47]. Further, the elastic properties of bones, muscles, and tissue in contact can be approximated as piecewise constant, but their actual values may vary from patient to patient. Knowing their exact characteristics can be used to reset, adjust, and finetune simulations [57]. This allows for better understanding of the biomechanical configuration at hand and therefore better, individualized treatment for every patient.

In [32], Ito and Kunisch suggested combining an output least squares and equation error formulation with the augmented Lagrangian method to solve inverse parameter estimation problems, an approach that has since become very successful; see, e.g., [16, 17, 19, 26, 40, 72]. Usually, these methods discretize the coefficients over the entire

*Submitted by the journal's Methods and Algorithms for Scientific Computing section May 18, 2011; accepted for publication (in revised form) January 2, 2013; published electronically April 16, 2013. This work was supported by the National Science Foundation under grants DMS-0502315, DMS-0652427, and CCF-0830554, by UC Lab Fees research grant DOE 09-LR-04-116741-BERA, and by the Office of Naval Research under grants ONR N000140310071 and ONR N000141010730.

<http://www.siam.org/journals/sisc/35-2/83450.html>

[†]Institute for Computational and Applied Mathematics, University of Münster, Einsteinstrasse 62, D-48149 Münster, Germany, and Department of Mathematics, University of California, Los Angeles, CA 90095-1555 (j.hegemann@uni-muenster.de).

[‡]Department of Mathematics, University of California, Los Angeles, CA 90095-1555 (cantarer@math.ucla.edu, jteran@math.ucla.edu). The work of the second author was supported by the National Science Foundation Graduate Research Fellowship under grant DGE-0707424.

[§]Center for Imaging Science, Johns Hopkins University, Baltimore, MD 21218 (clr@cis.jhu.edu). This author's work was partially supported by NSF grant DMS-0714945.

domain and use a total variation regularization to achieve an essentially piecewise constant solution for the coefficients. This, and the homogeneous structure of the coefficients in many applications, e.g., geophysical sciences [4, 39], inverse scattering [43], and medical imaging as mentioned before, is motivation to include the piecewise constant nature of the coefficients into the approach to these problems.

In addition to estimating the coefficients of a PDE, the geometry of the domain of interest is important for many applications, such as the locations of cavities within a material or an optimal shape design under certain exterior conditions. For this so-called inverse geometric problem, where the unknown is a geometric shape, many different approaches have been proposed, e.g., [28, 29, 30, 38, 39]. In [58], Santosa suggested the use of the level set method, developed by Osher and Sethian [53], for inverse obstacle problems. The implicit representation of an interface as the zero level set of a function allows for the natural handling of topology changes, such as splitting and merging. Therefore, the level set is capable of evolving toward a solution from almost any initial shape, requiring little or no a priori knowledge. This versatility is highly desirable for solving shape optimization and shape reconstruction problems since the topology of the solution is usually unknown; cf. [10, 11, 12, 13, 14, 23, 33, 52, 54, 55, 56, 63, 66, 67].

Much of the previous work has been done on the model inverse problem arising from Poisson's equation,

$$\begin{cases} -\nabla \cdot \beta \nabla u = f & \text{in } \Omega, \\ u = g_1 & \text{on } \partial\Omega_D, \\ \frac{\partial u}{\partial n} = g_2 & \text{on } \partial\Omega_N, \end{cases}$$

with applications ranging from electrical impedance tomography [9, 20, 63] and DC resistivity [61] to ground water and oil reservoir investigations [36, 37]. Some authors, e.g., [18, 22, 49, 65], have combined the two aforementioned approaches for the case of Poisson's equation. The goal of these papers is to recover the coefficients as well as the unknown interface.

There has been some work to extend these or similar techniques to the related elliptic inverse problem originating in linear elasticity,

$$\begin{cases} -\nabla \cdot \sigma(u) = f & \text{in } \Omega, \\ u = \bar{u} & \text{on } \partial\Omega_D, \\ \sigma \cdot n = \bar{t} & \text{on } \partial\Omega_N, \end{cases}$$

where

$$\begin{aligned} \sigma(u) &= 2\mu\epsilon(u) + \lambda \operatorname{tr}(\epsilon(u)) I, \\ \epsilon(u) &= \frac{1}{2}(\nabla u + \nabla u^T), \end{aligned}$$

with applications in material property determination and inclusion detection [41, 59] as well as design optimization [1, 2, 8, 15, 44, 60, 70] and medical imaging [31, 35]. The goal of these works has been either to estimate the Lamé parameters [24, 25, 34, 50] or to solve the inverse geometric problem [3, 7].

In the present paper, we also combine the augmented Lagrangian approach with the level set method. As opposed to the aforementioned work of [18], we do not use the

whole finite element space to approximate the coefficients in each element combined with a total variation regularization. That approach requires an additional nonlinear solve for the coefficients at every grid point at every iteration. The versatility of allowing the coefficients to spatially vary is typically dominated by the TV norm, which leads to smoothing of the solution and to essentially piecewise constant results.

Our approach incorporates the information about the nature of the piecewise constant coefficients directly into the method, which allows us to avoid the additional solve corresponding to the coefficients and instead obtain an explicit, and therefore very efficient, update at each iteration. Furthermore, we obtain the velocity for the level set evolution by use of the shape derivative of our objective functional, leading to an equally efficient update of the interface geometry.

The apparent limitation to truly piecewise constant coefficients is justified in many applications, where the materials are essentially homogeneous. Other authors have successfully included the assumption of piecewise constant coefficients into their approaches [21, 22, 49, 65]. However, our method uses a different objective functional and is more efficient because we use only one linear solve per iteration; all other variables are updated explicitly. For simplicity, we limit this paper to the example problems of Poisson's equation and linear elasticity, but the methodology is rather general and can be extended to other inverse problems constrained by linear elliptic PDEs.

2. Problem formulation. Let $\Omega \subset \mathbb{R}^d$ be open and bounded, with a smooth or piecewise smooth boundary $\partial\Omega$. We model two elliptic inverse problems: Poisson's equation as well as linear elasticity. Due to the ill-posedness of both inverse problems, we use output-least-squares with an observation $u_0 \in L^2(\Omega)$ of the solution to recover the unknown coefficients occurring in the respective PDE. We allow the coefficients to have jump discontinuities across some unknown interface Γ in Ω and recover Γ as well. This interface Γ , which separates the domain into two disjoint open sets, Ω_1 and Ω_2 , is assumed to be (piecewise) smooth and is represented implicitly by a level set function ϕ (for more details on the level set method, we refer the reader to [51]). The subsets Ω_1 and Ω_2 correspond to the regions of positive and negative function values of ϕ (see Figure 1):

$$\begin{aligned}\Omega_1 &= \{x \in \Omega | \phi(x) < 0\}, \\ \Omega_2 &= \{x \in \Omega | \phi(x) > 0\}, \\ \Gamma &= \{x \in \Omega | \phi(x) = 0\} = \partial\Omega_1 \setminus \partial\Omega = \partial\Omega_2 \setminus \partial\Omega.\end{aligned}$$

(The limitation to two regions is for simplicity only; a generalization to arbitrary numbers of subregions is easily obtainable via multiple level sets; see, e.g., [18, 64, 69].) We assume the coefficients to be constant in each Ω_i and denote the restriction of a value in one region by a subscript i .

2.1. Poisson's equation. We employ Poisson's equation as a first case to show the simplicity of our approach:

$$(1) \quad \begin{cases} -\nabla \cdot \beta \nabla u = f & \text{in } \Omega, \\ u = g & \text{on } \partial\Omega_D, \\ \frac{\partial u}{\partial n} = 0 & \text{on } \partial\Omega_N, \end{cases}$$

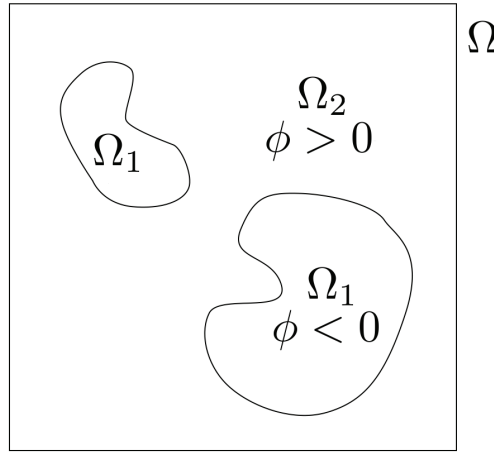


FIG. 1. *Problem setting: Two materials, represented by Ω_1 and Ω_2 , with different, unknown properties are in contact. The interface between them, where the parameters have a jump discontinuity, is unknown as well.*

with piecewise constant coefficient

$$(2) \quad \beta = \begin{cases} \beta_1 & \text{in } \Omega_1, \\ \beta_2 & \text{in } \Omega_2. \end{cases}$$

We solve the constrained minimization problem

$$(3) \quad \min_{\beta_1, \beta_2, \Gamma} \int_{\Omega} |u - u_0|^2 dx + w|\Gamma| \quad \text{such that } u \in H^1(\Omega) \text{ is a solution to (1),}$$

where $|\Gamma| = \mathcal{H}^{d-1}(\Gamma)$ denotes the $(d-1)$ -dimensional Hausdorff measure of Γ and $w > 0$ is a weighting parameter. The corresponding augmented Lagrangian functional for any $r > 0$ is defined as

$$(4) \quad \begin{aligned} \mathcal{L}_A(u, v, \beta_1, \beta_2, \Gamma; r, w) = & \frac{1}{2} \int_{\Omega} |u - u_0|^2 dx + \int_{\Omega} (\nabla v \cdot \beta \nabla u - fv) dx \\ & + \frac{r}{2} \int_{\Omega} |\nabla \cdot \beta \nabla u + f|^2 dx + w|\Gamma|. \end{aligned}$$

The use of the augmented Lagrangian framework, rather than a regular Lagrangian approach, is motivated by its superior stability properties for iterative schemes, especially in case of noise present in the observation u_0 (see, e.g., [16]). We find the saddle point of (4) by solving the first order optimality conditions:

$$(5) \quad \frac{\partial \mathcal{L}_A}{\partial u} = u - u_0 - \nabla \cdot \beta \nabla v + r \nabla \cdot \beta \nabla (\nabla \cdot \beta \nabla u + f) = 0,$$

$$(6) \quad \frac{\partial \mathcal{L}_A}{\partial \beta_i} = \int_{\Omega_i} \nabla v \cdot \nabla u dx + r \int_{\Omega_i} (\nabla \cdot \beta_i \nabla u + f) \Delta u dx = 0 \quad \text{for } i = 1, 2.$$

For the derivative with respect to the geometry, we use some classical results about shape derivatives, as given in Appendix A. In order to apply these lemmas, we split

the integral into the subsets Ω_i , yielding

$$(7) \quad \begin{aligned} \frac{\partial \mathcal{L}_A}{\partial \Omega}[\theta] &= \sum_{i=1}^2 \int_{\partial \Omega_i \setminus \partial \Omega} \left(\frac{1}{2}|u - u_0|^2 + \nabla u \cdot \beta_i \nabla v - fv + \frac{r}{2}|\nabla \cdot \beta_i \nabla u + f|^2 \right) \theta(x) \cdot n_i(x) ds \\ &\quad + w \int_{\partial \Omega_i \setminus \partial \Omega} \kappa_i(x) \theta(x) \cdot n_i(x) ds \\ &= 0, \end{aligned}$$

where n_i is the outside normal to Ω_i , and $\kappa_i = \nabla \cdot n_i$ is the mean curvature of $\partial \Omega_i$. Since $n_2 = -n_1$ on $\Gamma = \partial \Omega_1 \cap \partial \Omega_2$ and thus also $\kappa_2 = -\kappa_1$, we are left with the following equation that needs to vanish on the interface:

$$(8) \quad V = \nabla u \cdot (\beta_1 - \beta_2) \nabla v + w \kappa.$$

With A representing the operator $(-\nabla \cdot \beta \nabla)$, and since $A^* = A$ for this problem, we can rewrite (5) as

$$(9) \quad (rA^2 + I)u = u_0 - Av + rAf,$$

with the boundary conditions specified in (1).

2.2. Linear elasticity. We mainly focus on the identification of unknown interfaces and material parameters in the more complicated case of linear elasticity. The governing equations are given by

$$(10) \quad \begin{cases} -\nabla \cdot \sigma(u) = f & \text{in } \Omega, \\ u = \bar{u} & \text{on } \partial \Omega_D, \\ \sigma \cdot n = 0 & \text{on } \partial \Omega_N. \end{cases}$$

The displacement u and the associated stress $\sigma(u)$ are related by Hooke's law,

$$(11) \quad \sigma(u) = C : \epsilon(u) = 2\mu\epsilon(u) + \lambda \operatorname{tr}(\epsilon(u)) I,$$

where C is the fourth order elasticity tensor and the strain is given by

$$(12) \quad \epsilon(u) = \frac{\nabla u + \nabla u^T}{2}.$$

The Lamé coefficients

$$(13) \quad \mu = \frac{E}{2(1+\nu)},$$

$$(14) \quad \lambda = \frac{\nu E}{(1+\nu)(1-2\nu)}$$

depend on Young's modulus E and Poisson's ratio ν . We consider a piecewise homogeneous material, and thus μ and λ are piecewise constant and are defined analogously to (2). In our approach we solve for μ and λ but use (13) and (14) to recover the physically meaningful material parameters E and ν .

We have a similar constrained minimization problem,

$$(15) \quad \min_{\mu_1, \lambda_1, \mu_2, \lambda_2, \Gamma} \int_{\Omega} |u - u_0|^2 dx + w|\Gamma| \quad \text{such that } u \in [H^1(\Omega)]^2 \text{ is a solution to (10).}$$

Again, we define the corresponding augmented Lagrangian functional for any $r > 0$ as

$$(16) \quad \begin{aligned} \mathcal{L}_A(u, v, \mu_1, \lambda_1, \mu_2, \lambda_2, \Gamma; r, w) = & \frac{1}{2} \int_{\Omega} |u - u_0|^2 dx \\ & + \int_{\Omega} ((2\mu\epsilon(u) + \lambda \operatorname{tr}(\epsilon(u)) I) : \epsilon(v) - fv) dx \\ & + \frac{r}{2} \int_{\Omega} |\nabla \cdot \sigma(u) + f|^2 dx + w|\Gamma| \end{aligned}$$

and compute its optimality conditions,

$$(17) \quad \frac{\partial \mathcal{L}_A}{\partial u} = u - u_0 - \nabla \cdot \sigma(v) + r\nabla \cdot \sigma(\nabla \cdot \sigma(u) + f) = 0,$$

and for $i = 1, 2$,

$$(18) \quad \begin{aligned} \frac{\partial \mathcal{L}_A}{\partial \mu_i} = & 2 \int_{\Omega_i} \epsilon(u) : \epsilon(v) dx \\ & + 2r \left(\int_{\Omega_i} \nabla \cdot (2\mu_i \epsilon(u) + \lambda_i \operatorname{tr}(\epsilon(u)) I) \cdot (\nabla \cdot \epsilon(u)) dx \right. \\ & \left. + \int_{\Omega_i} f \cdot (\nabla \cdot \epsilon(u)) dx \right) \\ = & 0, \end{aligned}$$

$$(19) \quad \begin{aligned} \frac{\partial \mathcal{L}_A}{\partial \lambda_i} = & \int_{\Omega_i} \operatorname{tr}(\epsilon(u)) I : \epsilon(v) dx \\ & + r \left(\int_{\Omega_i} \nabla \cdot (2\mu_i \epsilon(u) + \lambda_i \operatorname{tr}(\epsilon(u)) I) \cdot (\nabla \cdot \operatorname{tr}(\epsilon(u)) I) dx \right. \\ & \left. + \int_{\Omega_i} f \cdot (\nabla \cdot \operatorname{tr}(\epsilon(u)) I) dx \right) \\ = & 0. \end{aligned}$$

Using the same argument and notation as before, the shape derivative in this case is given by

$$(20) \quad \begin{aligned} \frac{\partial \mathcal{L}_A}{\partial \Omega}[\theta] = & \sum_{i=1}^2 \int_{\partial \Omega_i \setminus \partial \Omega} \left(\frac{1}{2} |u - u_0|^2 + \epsilon(u) : C_i : \epsilon(v) - fv \right. \\ & \left. + \frac{r}{2} |\nabla \cdot \sigma_i(u) + f|^2 \right) \theta(x) \cdot n_i(x) ds + w \int_{\partial \Omega_i \setminus \partial \Omega} \kappa_i(x) \theta(x) \cdot n_i(x) ds \\ = & 0, \end{aligned}$$

yielding

$$(21) \quad V = \epsilon(u) : (C_1 - C_2) : \epsilon(v) + w\kappa,$$

which needs to vanish on the interface.

Again, using the corresponding linear operator $A = \nabla \cdot \sigma(\cdot)$, we obtain u by solving

$$(22) \quad (rA^2 + I)u = u_0 - Av + rAf$$

with the boundary conditions of the original problem (10).

For a more rigorous analysis of augmented Lagrangian methods for identifying discontinuous parameters in elliptic systems, we refer the interested reader to [19, 26]. For a detailed analysis of convergence of level set methods for elliptic inverse problems as well as a more general functional-analytic framework of level set methods and shape reconstruction, see [10, 11, 13].

3. Optimization algorithm. In order to solve the equations derived in the previous section, we use an alternating optimization algorithm. We denote the iterations by k and discretize all operators and functions in an appropriate manner.

3.1. Coefficient updates. For the coefficients, we use the optimality conditions to derive an explicit update rule (the complete derivations can be found in Appendix B). In the case of Poisson's equation, we assume $f \neq 0$ and solve (6) at iteration $k+1$ for β_i^{k+1} . Since β_i is constant on Ω_i , we can substitute $\Delta u = -\frac{f}{\beta_i^k}$ on the right-hand side, yielding

$$(23) \quad \beta_i^{k+1} = \beta_i^k - \frac{\int_{\Omega_i} \nabla v \cdot \nabla u dx}{r/(\beta_i^k)^2 \int_{\Omega_i} f^2 dx} \quad \text{for } i = 1, 2.$$

Similarly, for linear elasticity we solve (18) and (19) for the coefficients μ_i and λ_i and then substitute in their respective values from the previous iteration:

$$(24) \quad \mu_i^{k+1} = \mu_i^k - \frac{\int_{\Omega_i} \epsilon(u) : \epsilon(v) dx}{2r \int_{\Omega_i} |\nabla \cdot \epsilon(u)|^2 dx},$$

$$(25) \quad \lambda_i^{k+1} = \lambda_i^k - \frac{\int_{\Omega_i} \text{tr}(\epsilon(u)) I : \epsilon(v) dx}{r \int_{\Omega_i} |\nabla \cdot \text{tr}(\epsilon(u)) I|^2 dx}.$$

3.2. Interface update. As mentioned in section 2, we represent the interface Γ implicitly by the zero contour of a level set function ϕ . A natural choice for ϕ is the signed distance to the interface

$$(26) \quad \phi(x) = \begin{cases} \text{distance}(x, \Gamma), & x \in \text{interior of } \Gamma, \\ -\text{distance}(x, \Gamma), & x \in \text{exterior of } \Gamma. \end{cases}$$

We evolve ϕ throughout an artificial time $t \in \mathbb{R}^+$ toward a stationary point with respect to a given velocity field:

$$(27) \quad \frac{d\phi}{dt}(x(t), t) = \frac{\partial \phi}{\partial t} + \nabla \phi \cdot v = 0.$$

The velocity field v can be chosen as the descent direction of the objective functional, i.e., as defined in (4) and (16) for Poisson's equation and linear elasticity, respectively. The gradient descent direction can be achieved by setting

$$(28) \quad \theta(x) = -V(x)n(x)$$

in (7) and (20). Its normal component $\theta \cdot n$ can then be used as the advection velocity in the Hamilton–Jacobi equation

$$(29) \quad \frac{\partial \phi}{\partial t} - |\nabla \phi| V = 0,$$

where we also used $n = \frac{\nabla\phi}{|\nabla\phi|}$. This allows us to obtain the velocities given by (8) and (21), respectively. The level set evolution reaches its steady state once the optimality condition is fulfilled.

We use a semi-implicit finite difference scheme based on the approach by Vese and Chan (see [69]) to discretize the level set evolution (29), and we regularize the descent direction of the zero-isocountour by replacing $|\nabla\phi|$ with an approximation of the Dirac delta-distribution,

$$(30) \quad \frac{\partial\phi}{\partial t} - \delta_\epsilon(\phi)V = 0,$$

using the following C^∞ regularization of the delta-distribution:

$$(31) \quad \delta_\epsilon(x) = \frac{1}{\pi} \frac{\epsilon}{\epsilon^2 + x^2}.$$

Since it is known [5, 27] that the solution to (29) is not generally a signed distance function, and in order to keep ϕ from getting too flat or too steep, we reinitialize it from time to time as a signed distance function by a fast-sweeping step following [71]. One has to be careful not to reinitialize too often. Our inverse problems are ill-posed, and therefore the evolution is very slow and it might take a long time for a nodal value to change sign. By reinitializing too often, these small changes could be revoked. In our method, we reinitialize either when a certain percentage of nodal values of ϕ have changed signs or after a fixed number of iterations have passed since the last reinitialization. A different strategy is to reinitialize after the L_2 norm of ϕ has changed more than a given percentage.

3.3. Algorithm. We now outline our algorithm (see Figure 2). First, we initialize ϕ^0 with the initial guess for the interface, the coefficients $(\beta_i^0 \text{ or } \mu_i^0, \lambda_i^0)$, ($i = 1, 2$), respectively) with positive values and v^0 as a zero-vector. We also choose a fixed number of iterations *reinit_number* and a percentage *reinit_ratio* for the level set reinitialization condition, as well as initialize the helper variables *number_sign_changes* and *iterations_since_reinit* as zero.

Remarks.

(i) The update order for the different variables is not important. Given an order, it is most efficient to use the most recent values on hand to update the remaining variables.

(ii) Note that $(rA^2 + I)$ never has to be built explicitly; only its application is needed, which makes computations efficient. The matrix $(rA^2 + I)$ is obviously symmetric and positive definite, and therefore we can use a (preconditioned) conjugate gradient method or similar to solve the equation to obtain u . We need only one solve per iteration since both the Lagrange multiplier v and the coefficients are updated explicitly.

(iii) We discretize the equations using the finite element method (FEM). We embed the interface by piecewise linear approximation into each element. We then use the true area weights to assemble the FEM stiffness matrix A and evaluate the integration exactly on each partition.

4. Numerical examples. For all examples we use a regular triangle grid of the domain $\Omega = [0, 1]^2$ with uniform spacing $\Delta x = \Delta y = h = 1/256$. The PDE solves for u are completed using FEM. The time step of the level set evolution is fixed to $\Delta t = h$ and coincides with a minimizing step of the Lagrangian functional

```

Initialization
for all  $k$  do
  Solve  $(rA^2 + I)u^{k+1} = u_0 - Av^k + rAf$ 
   $v^{k+1} \leftarrow v^k + r(Au^{k+1} - f)$  // explicit update of the Lagrange multiplier
  for all  $i = 1$  to  $2$  do // explicit update of the coefficients
    // in case of Poisson's equation
     $\beta_i^{k+1} \leftarrow \beta_i^k - \frac{\int_{\Omega_i} \nabla v^{k+1} \cdot \nabla u^{k+1}}{r/(\beta_i^k)^2 \int_{\Omega_i} f^2}$ 
    or // in case of linear elasticity
     $\mu_i^{k+1} \leftarrow \mu_i^k - \frac{\int_{\Omega_i} \epsilon(u^{k+1}) : \epsilon(v^{k+1})}{2r \int_{\Omega_i} |\nabla \cdot \epsilon(u^{k+1})|^2}$ 
     $\lambda_i^{k+1} \leftarrow \lambda_i^k - \frac{\int_{\Omega_i} \text{tr}(\epsilon(u^{k+1})) I : \epsilon(v^{k+1})}{r \int_{\Omega_i} |\nabla \cdot \text{tr}(\epsilon(u^{k+1})) I|^2}$ 
  end for
  Advect( $\phi^k, \phi^{k+1}$ ) // as described in section 3.2
  for all  $i = 1$  to  $number\_nodes$  do // check  $\phi$  for a sign changes
    if  $\phi_i^k \cdot \phi_i^{k+1} < 0$  then
       $number\_sign\_changes \leftarrow number\_sign\_changes + 1$ 
    end if
  end for
  if  $iterations\_since\_reinit > reinit\_number$ 
  or  $number\_sign\_changes/number\_nodes > reinit\_ratio$  then
    Fast_sweep( $\phi^{k+1}$ ) // reinitialization as a signed distance function
     $number\_sign\_changes \leftarrow 0$ 
     $iterations\_since\_reinit \leftarrow 0$ 
  end if
  Check convergence based on
   $E_i \leftarrow \frac{\mu_i(3\lambda_i + 2\mu_i)}{\lambda_i + \mu_i}$ 
   $\nu_i \leftarrow \frac{\lambda_i}{2(\lambda_i + \mu_i)}$ 
  and the interface
end for

```

FIG. 2.

TABLE 1
Recovered coefficients for Poisson's equation.

Coefficient	Exact	Recovered	Relative error
β_1	5.0	5.00252	0.0504%
β_2	1.0	1.00089	0.089%

\mathcal{L}_A . For the approximation of the interface in (31), we set $\epsilon = h$. We reinitialize ϕ either when 10% of the vertices have changed sign or when 100 iterations have passed since the last reinitialization. The convergence is often very fast in the beginning of the computation and then slows down after an initial phase. This accounts for the high total number of iterations we observe and is typical for augmented Lagrangian methods; cf. [18].

4.1. Poisson's equation. We demonstrate our algorithm for the case of Poisson's equation using an example where Ω_1 is composed of two different shapes, a square and an ellipse, included in Ω . We choose the simple case of $f = 1$ and homogeneous boundary conditions. The exact solution is computed with $\beta_1 = 5.0$ and $\beta_2 = 1.0$, and we choose $r = 1.0$ and $w = 5 \cdot 10^{-6}$ and obtain a very accurate recovery

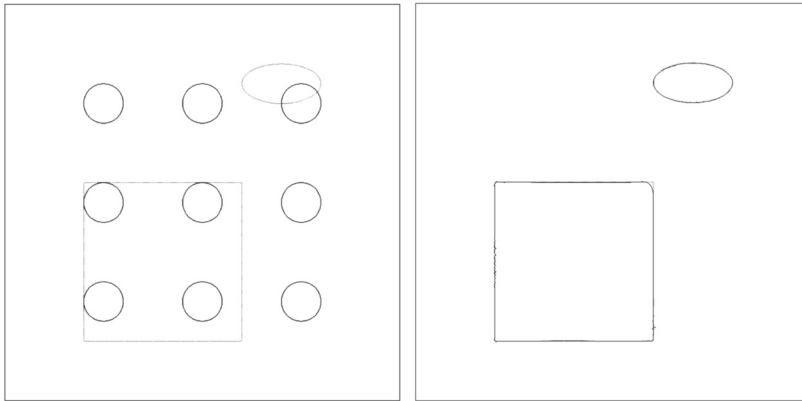


FIG. 3. *Interface recovery for Poisson's equation: exact solution with initial (left) and final configuration (right).*

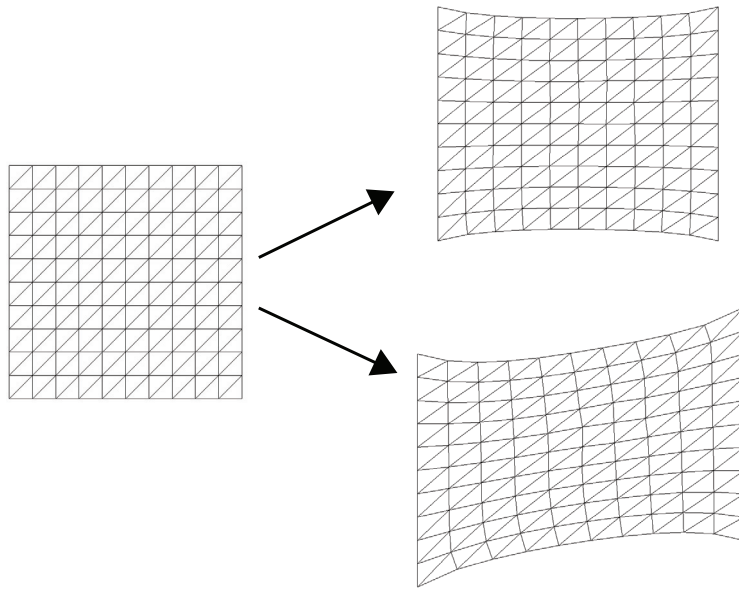


FIG. 4. *Illustration of the boundary displacements used in the examples: the undeformed domain on the left is deformed into the configuration on the right, either by pure stretching in the example "square and ellipse" (upper right) or by pulling and shearing in the example "elaborate geometry" (lower right). Note that the boundary displacements used in this picture are exaggerated for illustration purposes; the displacements used in the experiments are much smaller.*

of the coefficients and the interface; see Table 1 and Figure 3.

4.2. Linear elasticity. We focus our numerical experiments on examples in linear elasticity and present multiple settings: we use the same geometric setting as before, with and without the addition of uniformly distributed noise, and also employ a more elaborate geometry. For all these examples, f is set equal to zero.

4.2.1. Square and ellipse. For this example, we choose the same geometric setting as above, with Ω_1 being a square and an ellipse. The boundary conditions are given as pure stretching by $u = (-0.01, 0)$ on the left and $u = (0.01, 0)$ on the

TABLE 2
Recovered coefficients for linear elasticity example “square and ellipse.”

Coefficient	Exact	Recovered	Relative error
E_1	200.0	200.068	0.034%
ν_1	0.28	0.280609	0.2175%
E_2	117.0	117.547	0.4675%
ν_2	0.33	0.329976	0.0073%

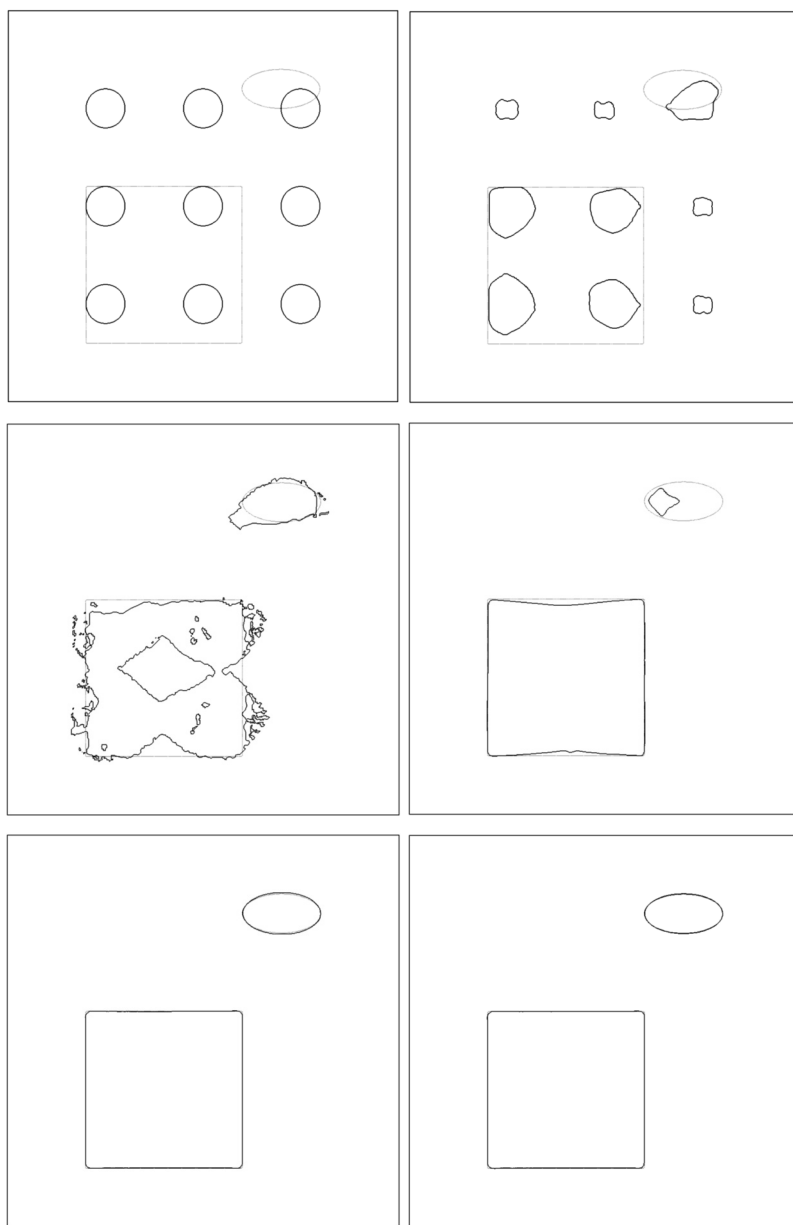


FIG. 5. *Interface evolution for linear elasticity example “square and ellipse” after 0, 1000, 2000, 5000, 10000, 12000 iterations (from top left to bottom right).*

TABLE 3

Recovered coefficients for linear elasticity example “square and ellipse,” with $\sigma = 5\%$ noise.

Coefficient	Exact	Recovered	Relative error
E_1	200.0	190.139	4.9305%
ν_1	0.28	0.280381	0.1361%
E_2	117.0	111.176	4.9778%
ν_2	0.33	0.330018	0.0055%

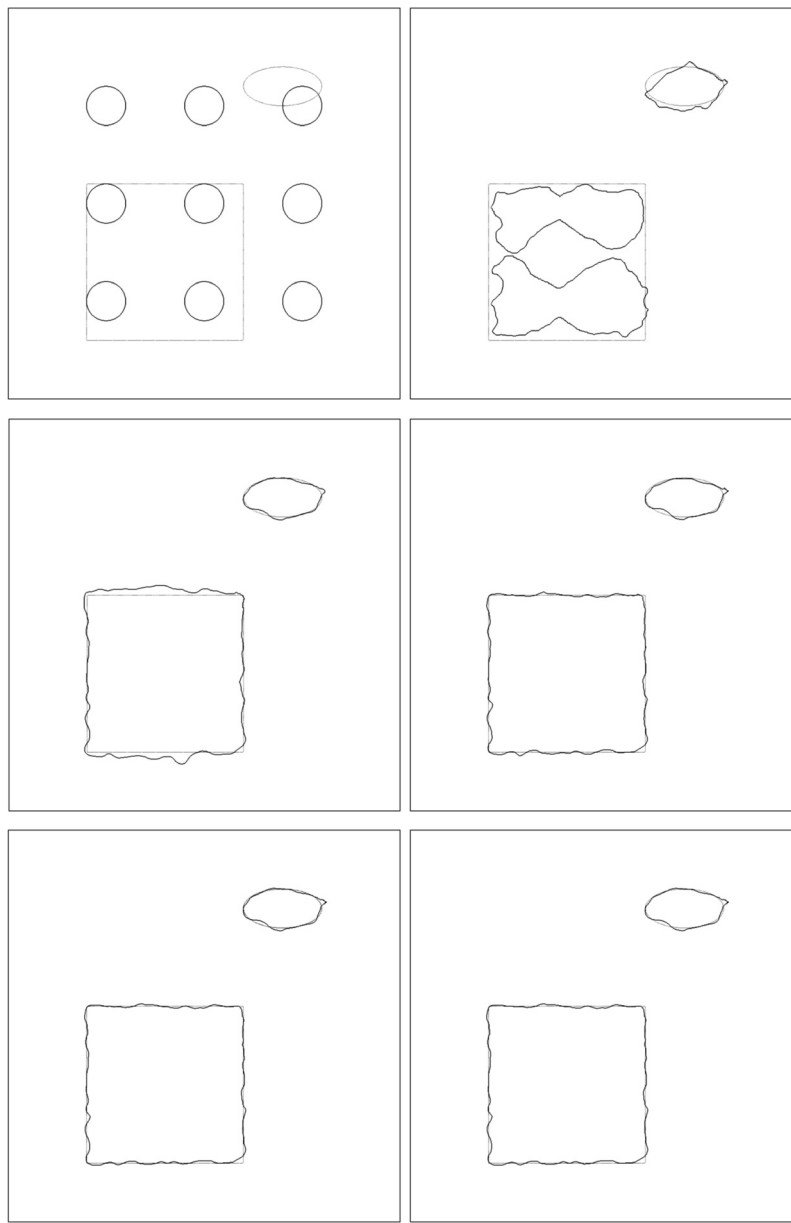


FIG. 6. Interface evolution for linear elasticity example “square and ellipse,” with $\sigma = 5\%$ noise, after 0, 1000, 3000, 5000, 10000, 13000 iterations (from top left to bottom right).

TABLE 4

Recovered coefficients for linear elasticity example “square and ellipse,” with $\sigma = 10\%$ noise.

Coefficient	Exact	Recovered	Relative error
E_1	200.0	221.334	10.6670%
ν_1	0.28	0.278046	0.6979%
E_2	117.0	129.226	10.4957%
ν_2	0.33	0.329707	0.0888%

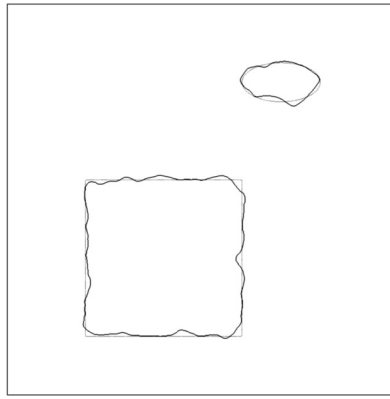
FIG. 7. *Recovered interface for linear elasticity example “square and ellipse,” with $\sigma = 10\%$ noise.*

TABLE 5

Recovered coefficients for linear elasticity example “square and ellipse,” with $\sigma = 20\%$ noise.

Coefficient	Exact	Recovered	Relative error
E_1	200.0	233.301	16.6505%
ν_1	0.28	0.274761	1.8711%
E_2	117.0	134.272	14.7624%
ν_2	0.33	0.330961	0.2912%

right, and free on top and bottom (see Figure 4 for an illustration). The material parameters are set to $E_1 = 200.0$, $\nu_1 = 0.28$ and $E_2 = 117.0$, $\nu_2 = 0.33$, for which we choose the initial guesses $E_1 = E_2 = 150.0$, $\nu_1 = \nu_2 = 0.30$. We choose $r = 0.001$, $w = 10^{-6}$ and are able to recover the coefficients (see Table 2) and the interface (see Figure 5 for the evolution) very accurately for this case.

4.2.2. Square and ellipse with noise. We now use the same settings as described above and add noise to the exact solution. We obtain our observation u_0 as follows:

$$u_0 = u^* + \sigma \frac{\|u^*\|_{L^2}}{\|S\|_{L^2}} S,$$

where u^* is the exact solution for a given set of coefficients. The vector S contains nodal values $s_i \in \mathbb{R}^d$, with $(s_i)_j \in [-1, 1]$ uniformly random, and σ controls the noise level. See Table 3 and Figure 6 for the results with $\sigma = 5\%$, $w = 10^{-5}$, and $r = 0.005$. Table 4 and Figure 7 show the results for $\sigma = 10\%$, $w = 2.0 \cdot 10^{-5}$, and $r = 0.005$, and the results of Table 5 and Figure 8 were computed with $\sigma = 20\%$, $w = 2.0 \cdot 10^{-5}$, and $r = 0.0075$.

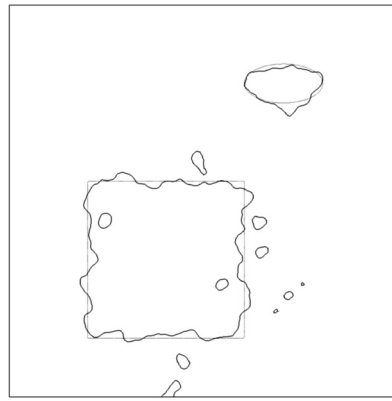


FIG. 8. Recovered interface for linear elasticity example “square and ellipse,” with $\sigma = 20\%$ noise.

TABLE 6
Recovered coefficients for linear elasticity example “elaborate geometry.”

Coefficient	Exact	Recovered	Relative error
E_1	200.0	207.974	3.9870%
ν_1	0.28	0.281306	0.4664%
E_2	117.0	121.568	3.9042%
ν_2	0.33	0.330681	0.2063%

4.2.3. Elaborate geometry. In our last example, we show that we can target a more complicated geometry, as shown in Figure 9 on the *left*. The material properties are given as in the previous example, but we change the initial guesses to $E_1 = 230.0$, $\nu_1 = 0.30$ and $E_2 = 80.0$, $\nu_2 = 0.35$. The boundary conditions are specified as $u = (-0.02, -0.01)$ on the left, $u = (0.02, 0.01)$ on the right, and free on top and bottom; i.e., we pull and shear the material (see Figure 4 for an illustration). For this example, we set $w = 10^{-5}$ and $r = 0.004$. The results can be seen in Table 6 and Figure 9 and show how accurately we can recover coefficients and interface even in this setting.

4.2.4. Elaborate geometry with noise. Just as before, we add different noise levels to this geometry. The results for $\sigma = 5\%$ (with $w = 10^{-4}$ and $r = 0.005$), $\sigma = 10\%$ (with $w = 2.0 \cdot 10^{-4}$ and $r = 0.005$), and $\sigma = 20\%$ (with $w = 2.0 \cdot 10^{-4}$ and $r = 0.005$) are presented in Tables 7–9 and Figures 10–12.

4.3. Parameter choices. Some words about the choice of the parameters r and w : It is well known that the weight on the interface length, w , controls its smoothness: high values can lead to an “oversmoothed” interface and even loss of smaller objects (see Figure 13 on the left), and small values can lead to jagged contours and small noise artifacts (see Figure 13 on the right). The augmented weight r needs to be large enough to ensure convergence, especially in the presence of noise. Choosing a larger r is always possible and can lead to better convergence in terms of total number of iterations, but at the price of higher computational cost per iteration due to its roll in (9) and (22), respectively. In fact, for most examples shown in this section we used very similar r -values for simplicity reasons and to demonstrate our ability to handle different observations with the same parameter.

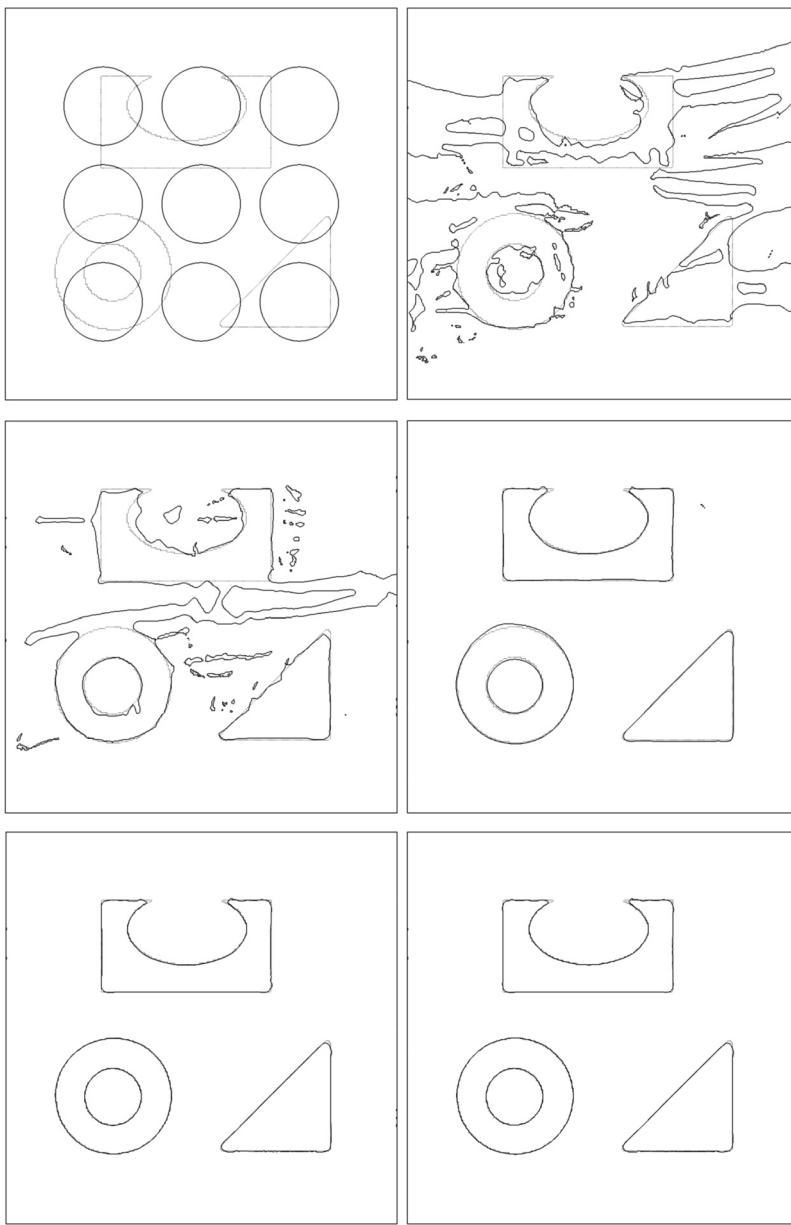


FIG. 9. Interface evolution for linear elasticity example “elaborate geometry” after 0, 1000, 2000, 3000, 4000, 5000 iterations (from top left to bottom right).

5. Conclusion. We have presented a fast, accurate, and easy-to-implement algorithm to solve for the arising coefficients as well as the discontinuity interface in elliptic PDEs, demonstrating it for the problems of Poisson’s equation and linear elasticity. The advantage of our approach is the treatment of the coefficients as truly piecewise constant. This provides us with a fast explicit update at every iteration since we only need one linear solve at every iteration; all other variables are updated explicitly, and we do not need an additional nonlinear solve. Further, our approach

TABLE 7

Recovered coefficients for linear elasticity example “elaborate geometry,” with $\sigma = 5\%$ noise.

Coefficient	Exact	Recovered	Relative error
E_1	200.0	211.515	5.7575%
ν_1	0.28	0.279285	0.2554%
E_2	117.0	123.206	5.3043%
ν_2	0.33	0.330886	0.2685%

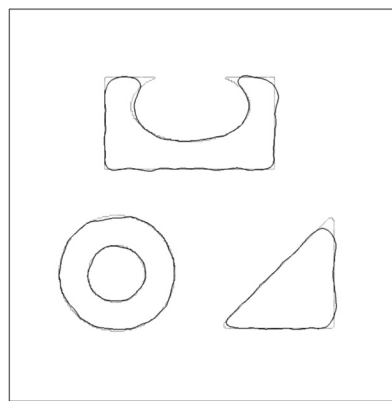


FIG. 10. *Recovered interface for linear elasticity example “elaborate geometry,” with $\sigma = 5\%$ noise.*

TABLE 8

Recovered coefficients for linear elasticity example “elaborate geometry,” with $\sigma = 10\%$ noise.

Coefficient	Exact	Recovered	Relative error
E_1	200.0	214.159	7.0795%
ν_1	0.28	0.271017	3.2082%
E_2	117.0	123.369	5.4436%
ν_2	0.33	0.33157	0.4758%

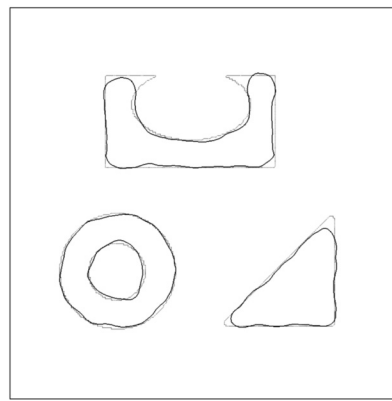


FIG. 11. *Recovered interface for linear elasticity example “elaborate geometry,” with $\sigma = 10\%$ noise.*

TABLE 9

Recovered coefficients for linear elasticity example “elaborate geometry,” with $\sigma = 20\%$ noise.

Coefficient	Exact	Recovered	Relative error
E_1	200.0	207.135	3.5675%
ν_1	0.28	0.268389	4.1468%
E_2	117.0	116.33	0.5727%
ν_2	0.33	0.330973	0.2948%

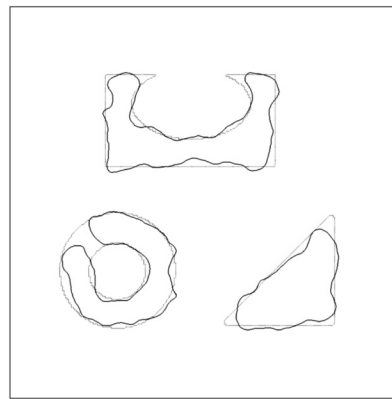


FIG. 12. Recovered interface for linear elasticity example “elaborate geometry,” with $\sigma = 20\%$ noise.

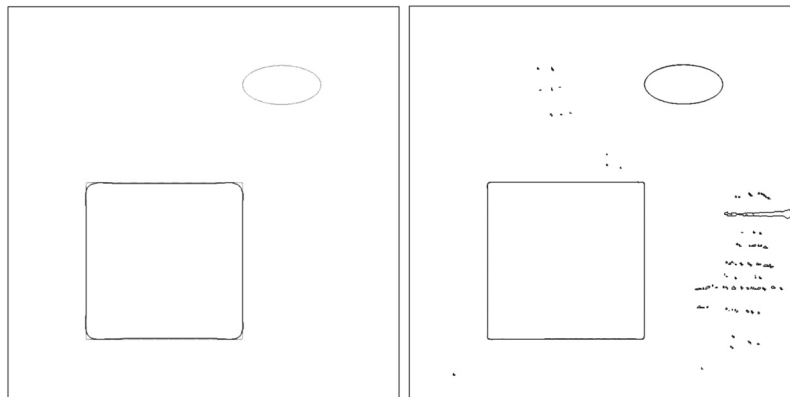


FIG. 13. Interfaces for linear elasticity example “square and ellipse” and different w -values: on the left, a high w -value leads to oversmoothing of the square and failure to detect the smaller ellipse to the upper right; on the right, a small w -value causes noisy artifacts.

is general and can be employed for any linear elliptic inverse problem. As presented in this paper, this allows us to provide the simultaneous recovery of coefficients and interface for Poisson’s equation and linear elasticity. For the case of Poisson’s equation we have to assume a nonzero right-hand side, but for linear elasticity the forcing term can be of any nature. Several numerical examples show that our method is numerically stable and can handle not only a variety of geometries but also a wide range of noise.

The essential difference between our method and previous work in the literature, e.g., [16, 17, 18], is that we reduce the computational cost per iteration from a nonlin-

ear solve, originating from the TV regularization, to an explicit update equation for the coefficients. Further, our method seems to be able to tolerate much higher noise levels than reported from those methods, especially for nontrivial interfaces. Some authors, like [33], can also deal with high observation error; however, they only solve for the interface and assume the constant coefficients to be known a priori.

Due to the ability of our method to handle input data polluted with noise, we expect it to work with experimental data. In the case of medical imaging, the interior measurement u_0 could be acquired by techniques involving ultrasound or MRI; see [35, 38, 46, 47, 57] and the references therein.

Currently, our method is based on a first order accurate solver on a triangular mesh. The incorporation of a second order method (cf. [6, 42, 68]) could potentially enhance every iteration. Also, a more advanced preconditioner, possibly based on multigrid methods (see [45] and the references therein), could further improve the runtime performance.

Appendix A. Shape derivatives. For completeness, we state some brief information about shape derivatives, which we use in section 2 to compute the derivatives of the energy functional with respect to the geometry. Following [2], we apply the subsequent statements (cf. [62]) in order to derive the correct speed for the interface evolution.

LEMMA 1. *Let $\Omega \subset \mathbb{R}^d$ be a smooth open set and let $\varphi \in W^{1,1}(\mathbb{R}^d)$. Then*

$$J(\Omega) := \int_{\Omega} \varphi(x) dx$$

is differentiable at Ω and

$$\begin{aligned} J'(\Omega)[\theta] &= \int_{\Omega} \nabla \cdot (\theta(x)\varphi(x)) dx \\ &= \int_{\partial\Omega} \theta(x) \cdot n(x) \varphi(x) ds \end{aligned}$$

for any $\theta \in W^{1,\infty}(\mathbb{R}^d; \mathbb{R}^d)$.

LEMMA 2. *Let $\Omega \subset \mathbb{R}^d$ be a smooth open set and let $\varphi \in W^{2,1}(\mathbb{R}^d)$. Then*

$$J(\Omega) := \int_{\partial\Omega} \varphi(x) ds$$

is differentiable at Ω and

$$J'(\Omega)[\theta] = \int_{\partial\Omega} \theta(x) \cdot n(x) \left(\frac{\partial \varphi}{\partial n}(x) + \varphi(x) \kappa(x) \right) ds$$

for any $\theta \in W^{1,\infty}(\mathbb{R}^d; \mathbb{R}^d)$, where $\kappa = \nabla \cdot n$ is the mean curvature of $\partial\Omega$.

Appendix B. Coefficient update. We now provide the derivative of the coefficient updates given in section 3.1.

For the case of Poisson's equation we start with (6) at iteration $k+1$ and assume that we already solved for $u = u^{k+1}$ and $v = v^{k+1}$. For a given $i \in \{1, 2\}$, β_i^{k+1} is constant over Ω_i , thus yielding

$$\begin{aligned} 0 &= \int_{\Omega_i} \nabla v \cdot \nabla u dx + r \int_{\Omega_i} (\nabla \cdot \beta_i^{k+1} \nabla u + f) \Delta u dx \\ \Rightarrow \beta_i^{k+1} &= \frac{- \int_{\Omega_i} \nabla v \cdot \nabla u dx}{r \int_{\Omega_i} (\Delta u)^2 dx} - \frac{\int_{\Omega_i} f \Delta u dx}{\int_{\Omega_i} (\Delta u)^2 dx} \end{aligned}$$

since we assume $f \neq 0$ for this case. While ∇u and ∇v can be evaluated numerically, we use a different approach for Δu . Since β_i is constant over Ω_i , we can write $\Delta u = -\frac{f}{\beta_i}$ within each region Ω_i . In this occurrence of the coefficient, we approximate it by its value from the previous iteration, yielding $\Delta u = -\frac{f}{\beta_i^k}$. This allows us to write an explicit update equation:

$$\begin{aligned}\beta_i^{k+1} &= -\frac{\int_{\Omega_i} \nabla v \cdot \nabla u dx}{r/(\beta_i^k)^2 \int_{\Omega_i} f^2 dx} + \beta_i^k \frac{\int_{\Omega_i} f^2 dx}{\int_{\Omega_i} f^2 dx} \\ &= \beta_i^k - \frac{\int_{\Omega_i} \nabla v \cdot \nabla u dx}{r/(\beta_i^k)^2 \int_{\Omega_i} f^2 dx}.\end{aligned}$$

For linear elasticity we first look at (18). Again, we use that the coefficient μ_i^{k+1} is constant over Ω_i , and thus

$$\begin{aligned}0 &= 2 \int_{\Omega_i} \epsilon(u) : \epsilon(v) dx \\ &\quad + 2r \left(\int_{\Omega_i} \nabla \cdot (2\mu_i^{k+1} \epsilon(u) + \lambda_i \text{tr}(\epsilon(u)) I) \cdot (\nabla \cdot \epsilon(u)) dx + \int_{\Omega_i} f \cdot (\nabla \cdot \epsilon(u)) dx \right) \\ \Rightarrow 2r\mu_i^{k+1} \int_{\Omega_i} |\nabla \cdot \epsilon(u)|^2 dx &= r \int_{\Omega_i} -\nabla \cdot (\lambda_i \text{tr}(\epsilon(u)) I - f) \cdot (\nabla \cdot \epsilon(u)) dx \\ &\quad - \int_{\Omega_i} \epsilon(u) : \epsilon(v) dx.\end{aligned}$$

Similarly to before, we use the PDE to substitute $2\mu_i \nabla \cdot \epsilon(u) = -\nabla \cdot \lambda_i \text{tr}(\epsilon(u)) I - f$ and use $\mu_i = \mu_i^k$ from the previous iteration for this term, allowing us to write

$$\begin{aligned}2r\mu_i^{k+1} \int_{\Omega_i} |\nabla \cdot \epsilon(u)|^2 dx &= 2\mu_i^k \int_{\Omega_i} |\nabla \cdot \epsilon(u)|^2 dx - \int_{\Omega_i} \epsilon(u) : \epsilon(v) dx \\ \Rightarrow \mu_i^{k+1} &= \mu_i^k - \frac{\int_{\Omega_i} \epsilon(u) : \epsilon(v) dx}{2r \int_{\Omega_i} |\nabla \cdot \epsilon(u)|^2 dx}.\end{aligned}$$

In the same way, (19) leads to

$$\begin{aligned}0 &= \int_{\Omega_i} \text{tr}(\epsilon(u)) I : \epsilon(v) dx \\ &\quad + r \left(\int_{\Omega_i} (\nabla \cdot (2\mu_i^{k+1} \epsilon(u) + \lambda_i \text{tr}(\epsilon(u)) I) - f) \cdot (\nabla \cdot \text{tr}(\epsilon(u)) I) dx \right) \\ \Rightarrow \lambda_i^{k+1} r \int_{\Omega_i} |\nabla \cdot \text{tr}(\epsilon(u)) I|^2 dx &= r \int_{\Omega_i} (-\nabla \cdot (2\mu_i \epsilon(u)) - f) \cdot (\nabla \cdot \text{tr}(\epsilon(u)) I) dx \\ &\quad - \int_{\Omega_i} \text{tr}(\epsilon(u)) I : \epsilon(v) dx.\end{aligned}$$

This time, we use $\lambda_i \nabla \cdot \text{tr}(\epsilon(u)) I = -\nabla \cdot (2\mu_i \epsilon(u)) - f$ from the original problem, with

$\lambda_i = \lambda_i^k$ for this occurrence:

$$\begin{aligned} \lambda_i^{k+1} r \int_{\Omega_i} |\nabla \cdot \text{tr}(\epsilon(u)) I|^2 dx &= r \int_{\Omega_i} (-\nabla \cdot (2\mu_i \epsilon(u)) - f) \cdot (\nabla \cdot \text{tr}(\epsilon(u)) I) dx \\ &\quad - \int_{\Omega_i} \text{tr}(\epsilon(u)) I : \epsilon(v) dx \\ \Rightarrow \lambda_i^{k+1} &= \lambda_i^k - \frac{\int_{\Omega_i} \text{tr}(\epsilon(u)) I : \epsilon(v) dx}{r \int_{\Omega_i} |\nabla \cdot \text{tr}(\epsilon(u)) I|^2 dx}. \end{aligned}$$

REFERENCES

- [1] G. ALLAIRE, F. JOUVE, AND A.M. TOADER, *A level-set method for shape optimization*, C. R. Math. Acad. Sci. Paris, 334 (2002), pp. 1125–1130.
- [2] G. ALLAIRE, F. JOUVE, AND A.M. TOADER, *Structural optimization using sensitivity analysis and a level-set method*, J. Comput. Phys., 194 (2004), pp. 363–393.
- [3] D. ALVAREZ, O. DORN, AND M. MOSCOSO, *A new level-set technique for the crack-detection problem*, Proc. Appl. Math. Mech., 7 (2007), pp. 1081501–1081502.
- [4] U. ASCHER AND E. HABER, *Computational methods for large distributed parameter estimation problems with possible discontinuities*, in Proceedings of the Symposium on Inverse Problems, Design, and Optimization, 2004, pp. 201–208.
- [5] G. BARLES, H.M. SONER, AND P.E. SOUGANIDIS, *Front propagation and phase field theory*, SIAM J. Control Optim., 31 (1993), pp. 439–469.
- [6] J. BEDROSSIAN, J.H. VON BRECHT, S. ZHU, E. SIFAKIS, AND J.M. TERAN, *A second order virtual node method for elliptic problems with interfaces and irregular domains*, J. Comput. Phys., 229 (2010), pp. 6405–6426.
- [7] H. BEN AMEUR, M. BURGER, AND B. HACKL, *Level set methods for geometric inverse problems in linear elasticity*, Inverse Problems, 20 (2004), pp. 673–696.
- [8] M.P. BENDSØE AND O. SIGMUND, *Topology Optimization: Theory, Methods, and Applications*, Springer-Verlag, Berlin, 2003.
- [9] L. BORCEA, G.A. GRAY, AND Y. ZHANG, *Variationally constrained numerical solution of electrical impedance tomography*, Inverse Problems, 19 (2003), pp. 1159–1184.
- [10] M. BURGER, *A level set method for inverse problems*, Inverse Problems, 17 (2001), pp. 1327–1355.
- [11] M. BURGER, *A framework for the construction of level set methods for shape optimization and reconstruction*, Interfaces Free Bound., 5 (2003), pp. 301–330.
- [12] M. BURGER, *Levenberg–Marquardt level set methods for inverse obstacle problems*, Inverse Problems, 20 (2004), pp. 259–282.
- [13] M. BURGER, N. MATEVOSYAN, AND M.T. WOLFRAM, *A level set based shape optimization method for an elliptic obstacle problem*, Math. Models Methods Appl. Sci., 21 (2011), pp. 619–649.
- [14] M. BURGER AND S.J. OSHER, *A survey on level set methods for inverse problems and optimal design*, European J. Appl. Math., 16 (2005), pp. 263–301.
- [15] V.J. CHALLIS, A.P. ROBERTS, AND A.H. WILKINS, *Fracture resistance via topology optimization*, Struct. Multidiscip. Optim., 36 (2008), pp. 263–271.
- [16] T.F. CHAN AND X.-C. TAI, *Augmented Lagrangian and total variation methods for recovering discontinuous coefficients from elliptic equations*, in Computational Science for the 21st Century. Symposium, 1997, pp. 597–607.
- [17] T.F. CHAN AND X.-C. TAI, *Identification of discontinuous coefficients in elliptic problems using total variation regularization*, SIAM J. Sci. Comput., 25 (2003), pp. 881–904.
- [18] T.F. CHAN AND X.-C. TAI, *Level set and total variation regularization for elliptic inverse problems with discontinuous coefficients*, J. Comput. Phys., 193 (2004), pp. 40–66.
- [19] Z. CHEN AND J. ZOU, *An augmented Lagrangian method for identifying discontinuous parameters in elliptic systems*, SIAM J. Control Optim., 37 (1999), pp. 892–910.
- [20] M. CHENEY, D. ISAACSON, AND J.C. NEWELL, *Electrical impedance tomography*, SIAM Rev., 41 (1999), pp. 85–101.
- [21] E.T. CHUNG, T.F. CHAN, AND X.-C. TAI, *Electrical impedance tomography using level set representation and total variational regularization*, J. Comput. Phys., 205 (2005), pp. 357–372.

- [22] A. DECEZARO, A. LEITÃO, AND X.-C. TAI, *On multiple level-set regularization methods for inverse problems*, Inverse Problems, 25 (2009), 035004.
- [23] O. DORN AND D. LESSELIER, *Level set methods for inverse scattering*, Inverse Problems, 22 (2006), pp. R67–R131.
- [24] M.S. GOCKENBACH, B. JADAMBA, AND A.A. KHAN, *Equation error approach for elliptic inverse problems with an application to the identification of Lamé parameters*, Inverse Problems Sci. Engrg., 16 (2008), pp. 349–367.
- [25] M.S. GOCKENBACH AND A.A. KHAN, *An abstract framework for elliptic inverse problems: Part 1. An output least-squares approach*, Math. Mech. Solids, 12 (2007), pp. 259–276.
- [26] M.S. GOCKENBACH AND A.A. KHAN, *An abstract framework for elliptic inverse problems: Part 2. An augmented Lagrangian approach*, Math. Mech. Solids, 14 (2009), pp. 517–539.
- [27] J. GOMES AND O. FAUGERAS, *Level sets and distance functions*, in Proceedings of the European Conference on Computer Vision (ECCV 2000), 2000, pp. 588–602.
- [28] F. HETTLICH AND W. RUNDELL, *Iterative methods for the reconstruction of an inverse potential problem*, Inverse Problems, 12 (1996), pp. 251–266.
- [29] F. HETTLICH AND W. RUNDELL, *Recovery of the support of a source term in an elliptic differential equation*, Inverse Problems, 13 (1997), pp. 959–976.
- [30] F. HETTLICH AND W. RUNDELL, *The determination of a discontinuity in a conductivity from a single boundary measurement*, Inverse Problems, 14 (1998), pp. 67–82.
- [31] C. HOGEA, C. DAVATZIKOS, AND G. BIROS, *An image-driven parameter estimation problem for a reaction-diffusion glioma growth model with mass effects*, J. Math. Biol., 56 (2008), pp. 793–825.
- [32] K. ITO AND K. KUNISCH, *The augmented Lagrangian method for parameter estimation in elliptic systems*, SIAM J. Control Optim., 28 (1990), pp. 113–136.
- [33] K. ITO, K. KUNISCH, AND Z. LI, *Level-set function approach to an inverse interface problem*, Inverse Problems, 17 (2001), pp. 1225–1242.
- [34] B. JADAMBA, A.A. KHAN, AND F. RACITI, *On the inverse problem of identifying Lamé coefficients in linear elasticity*, Comput. Math. Appl., 56 (2008), pp. 431–443.
- [35] L. JI, J.R. McLAUGHLIN, D. RENZI, AND J.R. YOON, *Interior elastodynamics inverse problems: Shear wave speed reconstruction in transient elastography*, Inverse Problems, 19 (2003), pp. S1–S29.
- [36] I. KNOWLES, *Parameter identification for elliptic problems*, J. Comput. Appl. Math., 131 (2001), pp. 175–194.
- [37] I. KNOWLES, T. LE, AND A. YAN, *On the recovery of multiple flow parameters from transient head data*, J. Comput. Appl. Math., 169 (2004), pp. 1–15.
- [38] V. KOLEHMAINEN, S.R. ARRIDGE, W.R.B. LIONHEART, M. VAUHKONEN, AND J.P. KAIPIO, *Recovery of region boundaries of piecewise constant coefficients of an elliptic PDE from boundary data*, Inverse Problems, 15 (1999), pp. 1375–1391.
- [39] K. KUNISCH AND X. PAN, *Estimation of interfaces from boundary measurements*, SIAM J. Control Optim., 32 (1994), pp. 1643–1674.
- [40] K. KUNISCH AND X.-C. TAI, *Sequential and parallel splitting methods for bilinear control problems in Hilbert spaces*, SIAM J. Numer. Anal., 34 (1997), pp. 91–118.
- [41] H.S. LEE, C.J. PARK, AND H.W. PARK, *Identification of geometric shapes and material properties of inclusions in two-dimensional finite bodies by boundary parameterization*, Comput. Methods Appl. Mech. Engrg., 181 (2000), pp. 1–20.
- [42] R.J. LEVEQUE AND Z. LI, *The immersed interface method for elliptic equations with discontinuous coefficients and singular sources*, SIAM J. Numer. Anal., 31 (1994), pp. 1019–1044.
- [43] A. LITMAN, D. LESSELIER, AND F. SANTOSA, *Reconstruction of a two-dimensional binary obstacle by controlled evolution of a level-set*, Inverse Problems, 14 (1998), pp. 685–706.
- [44] Z. LUO, L. TONG, J. LUO, P. WEI, AND M.Y. WANG, *Design of piezoelectric actuators using a multiphase level set method of piecewise constants*, J. Comput. Phys., 228 (2009), pp. 2643–2659.
- [45] A. MCADAMS, E. SIFAKIS, AND J. TERAN, *A parallel multigrid Poisson solver for fluids simulation on large grids*, in Proceedings of the 2010 ACM SIGGRAPH/Eurographics Symposium on Computer Animation, Eurographics Association, 2010, pp. 65–74.
- [46] J. McLAUGHLIN AND D. RENZI, *Using level set based inversion of arrival times to recover shear wave speed in transient elastography and supersonic imaging*, Inverse Problems, 22 (2006), pp. 707–725.
- [47] J.R. McLAUGHLIN, N. ZHANG, AND A. MANDUCA, *Calculating tissue shear modulus and pressure by 2D log-elastographic methods*, Inverse Problems, 26 (2010), 085007.
- [48] F. NATTERER, *Imaging and Inverse Problems of Partial Differential Equations*, preprint, University Münster, 2006.

- [49] L.K. NIELSEN, X.-C. TAI, S.I. AANONSEN, AND M. ESPEDAL, *A binary level set model for elliptic inverse problems with discontinuous coefficients*, Int. J. Numer. Anal. Model., 4 (2007), pp. 74–99.
- [50] A.A. OBERAI, N.H. GOKHALE, AND G.R. FEIJÓO, *Solution of inverse problems in elasticity imaging using the adjoint method*, Inverse Problems, 19 (2003), pp. 297–313.
- [51] S. OSHER AND R. FEDKIW, *Level Set Methods and Dynamic Implicit Surfaces*, Springer-Verlag, New York, 2002.
- [52] S.J. OSHER AND F. SANTOSA, *Level set methods for optimization problems involving geometry and constraints I. Frequencies of a two-density inhomogeneous drum*, J. Comput. Physics, 171 (2001), pp. 272–288.
- [53] S. OSHER AND J.A. SETHIAN, *Fronts propagating with curvature-dependent speed: Algorithms based on Hamilton-Jacobi formulations*, J. Comput. Physics, 79 (1988), pp. 12–49.
- [54] C. RAMANANJAONA, M. LAMBERT, AND D. LESSELIER, *Shape inversion from TM and TE real data by controlled evolution of level sets*, Inverse Problems, 17 (2001), pp. 1585–1595.
- [55] C. RAMANANJAONA, M. LAMBERT, D. LESSELIER, AND J.P. ZOLÉSIO, *Shape reconstruction of buried obstacles by controlled evolution of a level set: From a min-max formulation to numerical experimentation*, Inverse Problems, 17 (2001), pp. 1087–1111.
- [56] C. RAMANANJAONA, M. LAMBERT, D. LESSELIER, AND J.P. ZOLÉSIO, *On novel developments of controlled evolution of level sets in the field of inverse shape problems*, Radio Science, 37 (2002), p. 8010.
- [57] A.P. SANTHANAM, Y. MIN, S.P. MUDUR, A. RASTOGI, B.H. RUDDY, A. SHAH, E. DIVO, A. KASSAB, J.P. ROLLAND, AND P. KUPELIAN, *An inverse hyper-spherical harmonics-based formulation for reconstructing 3D volumetric lung deformations*, Comptes Rendus Mécanique, 338 (2010), pp. 461–473.
- [58] F. SANTOSA, *A level-set approach for inverse problems involving obstacles*, ESAIM Contrôl Optim. Calc. Var., 1 (1996), pp. 17–33.
- [59] D.S. SCHNUR AND N. ZABARAS, *An inverse method for determining elastic material properties and a material interface*, Internat. J. Numer. Methods Engrg., 33 (1992), pp. 2039–2057.
- [60] J.A. SETHIAN AND A. WIEGMANN, *Structural boundary design via level set and immersed interface methods*, J. Comput. Phys., 163 (2000), pp. 489–528.
- [61] N.C. SMITH AND K. VOZOFF, *Two-dimensional DC resistivity inversion for dipole-dipole data*, IEEE Trans. Geosci. Remote Sensing, GE-22 (1984), pp. 21–28.
- [62] J. SOKOLOWSKI AND J.P. ZOLESI, *Introduction to Shape Optimization: Shape Sensitivity Analysis*, Springer-Verlag, Berlin, 1992.
- [63] M. SOLEMANI, W.R.B. LIONHEART, AND O. DORN, *Level set reconstruction of conductivity and permittivity from boundary electrical measurements using experimental data*, Inverse Problems Sci. Engrg., 14 (2006), pp. 193–210.
- [64] X.-C. TAI AND T.F. CHAN, *A survey on multiple level set methods with applications for identifying piecewise constant functions*, Int. J. Numer. Anal. Model., 1 (2004), pp. 25–48.
- [65] X.-C. TAI AND H. LI, *A piecewise constant level set method for elliptic inverse problems*, Appl. Numer. Math., 57 (2007), pp. 686–696.
- [66] K. VAN DEN DOEL AND U.M. ASCHER, *On level set regularization for highly ill-posed distributed parameter estimation problems*, J. Comput. Phys., 216 (2006), pp. 707–723.
- [67] K. VAN DEN DOEL, U.M. ASCHER, AND A. LEITAO, *Multiple level sets for piecewise constant surface reconstruction in highly ill-posed problems*, J. Sci. Comput., 43 (2010), pp. 44–66.
- [68] B.L. VAUGHAN, B.G. SMITH, AND D.L. CHOPP, *A comparison of the extended finite element method with the immersed interface method for elliptic equations with discontinuous coefficients and singular sources*, Appl. Math. Comput. Sci., 1 (2006), pp. 207–228.
- [69] L.A. VESE AND T.F. CHAN, *A multiphase level set framework for image segmentation using the Mumford and Shah model*, Internat. J. Comput. Vision, 50 (2002), pp. 271–293.
- [70] P. WEI AND M.Y. WANG, *Piecewise constant level set method for structural topology optimization*, Internat. J. Numer. Methods Engrg., 78 (2009), pp. 379–402.
- [71] H. ZHAO, *A fast sweeping method for eikonal equations*, Math. Comp., 74 (2005), pp. 603–628.
- [72] J. ZOU, *Numerical methods for elliptic inverse problems*, Int. J. Comput. Math., 70 (1998), pp. 211–232.